CHEMISTRY OF MATERIALS

ARTICLE

pubs.acs.org/cm

High-Performance Stable *n*-Type Indenofluorenedione Field-Effect Transistors

Young-Il Park,[†,⊥] Joong Suk Lee,[‡,⊥] Beom Joon Kim,[‡] Beomjin Kim,[†] Jaehyun Lee,[†] Do Hwan Kim,[§] Se-Young Oh,[▽] Jeong Ho Cho,[*,‡] and Jong-Wook Park[*,†]

[†]Department of Chemistry/Display Research Center, The Catholic University of Korea, Bucheon 420-743, Republic of Korea

[‡]Department of Organic Materials and Fiber Engineering, Soongsil University, Seoul 156-743, Republic of Korea

[§]Department of Chemical Engineering, Stanford University, 381 North-South Mall, Stanford, California 94305, United States

[▽]Department of Chemical and Biomolecular Engineering, Sogang University, Seoul 121-742, Republic of Korea

Supporting Information

ABSTRACT: We developed high-performance stable *n*-type organic field-effect transistors (OFETs) using indenofluorenediones with different numbers of fluorine substituents (MonoF-IF-dione, DiF-IF-dione, and TriF-IF-dione). Top-contact OFETs were fabricated via the vacuum deposition of indenofluorenediones as the semiconducting channel material on polystyrene-treated SiO_2/Si substrates. TriF-IF-dione FETs with Au source/drain contacts exhibited good device performances, with a field-effect mobility of 0.16 $cm^2/(V\,s)$, an on/off current ratio of 10^6, and a threshold voltage of 9.2 V. We found that the electrical stability for OFETs based on indenofluorenedione improved with the number of fluorine substituents, which was attributed to higher activation energies for charge trap creation. Moreover, the TriF-IF-dione FETs yielded excellent environmental stability properties, because the LUMO energy levels were relatively low, compared with those of the MonoF-IF-dione FETs.

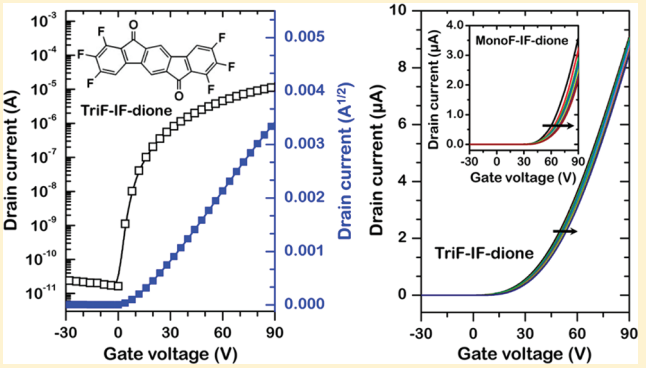

KEYWORDS: indenofluorenedione, n-type field-effect transistors (FETs), fluorine substituent, electrical stability, environmental stability

1. INTRODUCTION

Organic field-effect transistors (OFETs) have recently attracted significant attention, because of their use in flexible large-area active display backplanes.[1−8] Demand for large-area flexible OFETs has driven significant interest in new types of solution-processable organic electronic materials, such as electrodes, insulators, and semiconductors. In addition to optimizing the gate dielectrics and electrode materials, the choice of high-performance solution-processable active semiconductors is very important for improving OFET performance.[9−11] Both *n*-type and *p*-type organic semiconductors are essential for *p*−*n* junction diodes, bipolar transistors, and complementary circuits that offer lower power consumption, higher operating speeds, and high noise tolerance margins.[12−17] However, most OFET-based circuits have been limited to *p*-type circuits, because of problems with *n*-type semiconductors, such as low mobility, intrinsic instabilities, and rapid degradation upon exposure to air.[18−23] Therefore, the development of high-mobility and environmentally stable *n*-type semiconducting materials is crucial for enabling the development of powerful complementary circuit technologies on flexible substrates.

n-Type organic semiconductors with high electron mobility have been demonstrated, including fullerene and its derivatives, perylene and naphthalene diimides, and substituted oligothiophene derivatives.[24−28] Recently, strong electron-withdrawing substituents, such as cyano, fluoro, and perfluoroalkyl, were introduced onto the π-conjugated cores to obtain air-stable *n*-type semiconductors by lowering the lowest unoccupied molecular orbital (LUMO) level. Several air-stable *n*-type semiconductors have been reported, such as perfluorinated metal phthalocyanine, fluoroacyl oligothiophenes, fluorocarbon-substituted naphthalene diimides, and cyano-substituted perylene diimides.[27,29−34] However, developing organic *n*-type semiconductors with both high mobility and good stability in air still remains a challenge. Another *n*-type semiconductor candidate for this purpose is indenofluorenedione, because the molecular structures of the pentacyclic diones are completely planar and form face-to-face π-stacking structures in the crystal.[35] Another advantage of indenofluorenedione is that substituents can be easily introduced. Therefore, in an effort to develop

Received: June 14, 2011
Revised: August 7, 2011
Published: August 19, 2011

Scheme 1. Synthesis of MonoF-IF-dione, DiF-IF-dione, and TriF-IF-dione

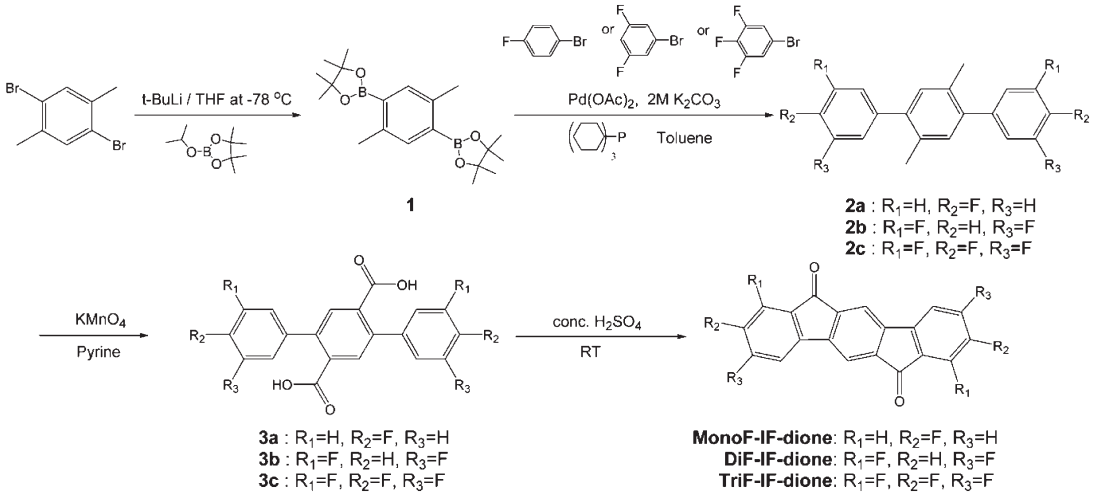

Scheme 2. Structures of MonoF-IF-dione, DiF-IF-dione, and TriF-IF-dione

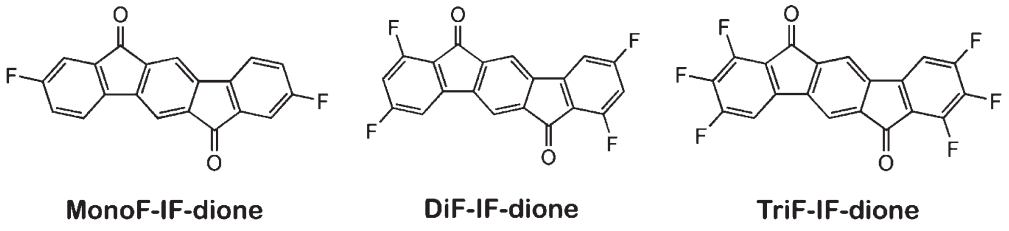

high-performance *n*-type semiconductors with good air stability, indenofluorenedione derivatives were synthesized. F atoms were introduced to the indenofluorenedione moiety to increase the electron affinity and lower the LUMO level according to the electron-withdrawing properties of fluorine. The influence of the number of substituted F atoms on the semiconductor crystalline nanostructure and electrical performance were also investigated.

To this end, indenofluorenediones with different numbers of fluorine substituents were synthesized and tested as high-performance stable *n*-type OFETs. The electronic properties of the synthesized compounds were investigated by cyclic voltammetry and ultraviolet−visible light (UV−vis) spectroscopy. TriF-IF-dione FETs with Au contacts fabricated on a polystyrene (PS) film exhibited excellent device performance, with a field-effect mobility of 0.16 $cm^2/(V\ s)$, an on/off current ratio of 10^6, and a threshold voltage of 9.2 V. The electrical and environmental stabilities of OFETs were also investigated. The electrical stabilities of OFETs were dramatically enhanced by the introduction of indenofluorenediones with higher numbers of fluorine substituents, because of the higher activation energies for charge trap creation. Moreover, TriF-IF-dione FETs yielded excellent environmental stability, compared with the MonoF-IF-dione FETs because fluorination was used to induce stability in the organic semiconductors by lowering the LUMO levels.

2. EXPERIMENTAL SECTION

2.1. Synthesis. The synthetic route and chemical structures of compounds used in this study are shown in Schemes 1 and 2. Synthetic details of the preparation of **2a**, **3a**, and MonoF-IF-dione have been described previously.[35,36]

Synthesis of Compound ***1***. 1,4-Dibromo-2,5-dimethyl-benzene (5 g, 18.9 mmol) was added to 200 mL of a tetrahydrofuran (THF) anhydrous solution and stirred at −78 °C, then 1.5 M *t*-BuLi (43 mL) was added. Isopropoxy-4,4,5,5-tetramethyl-1,3,2-dioxaborolane (9.2 mL, 45.3 mmol) was then added to the reaction mixture after 1 h. After the reaction had finished, the reaction mixture was extracted with ethyl acetate and water. The organic layer was dried with anhydrous $MgSO_4$ and filtered. The solvent was removed by evaporation. Recrystallization of the residue from ethyl acetate/MeOH afforded a white product: 80% yield, ^{1}H NMR (300 MHz, $CDCl_3$): 7.53(s, 2H), 2.47(s, 6H), 1.33(s, 24H).

Synthesis of Compound ***2b***. Compound **1** (1.5 g, 4.18 mmol), 1-bromo-3,5-difluoro-benzene (1.78 g, 9.22 mmol), $Pd(OAc)_2$ (0.02 g, 0.10 mmol), and tricyclohexylphosphine (0.05 g, 0.21 mmol) were added to 50 mL of toluene, then 10 mL of 2 M K_2CO_3 was added to the reaction mixture. The mixture was heated to 70 °C for 6 h under nitrogen. After the reaction was complete, the reaction mixture was extracted with chloroform and water. The organic layer was dried with anhydrous $MgSO_4$ and filtered. The solvent was removed by evaporation. Recrystallization of the residue from $CHCl_3$/MeOH afforded a white product: 47% yield, ^{1}H NMR (300 MHz, DMSO-d_6): 7.27−7.18(m, 4H), 7.12−7.08(m, 4H), 2.22(s, 6H).

Synthesis of Compound ***2c***. Compound **1** (1.5 g, 7.1 mmol), 5-bromo-1,2,3-trifluoro-benzene (3.3 g, 15.6 mmol), $Pd(OAc)_2$ (0.04 g, 0.21 mmol), and tricyclohexylphosphine (0.11 g, 0.42 mmol) were added to 100 mL of toluene, then 20 mL of 2 M K_2CO_3 was added to the reaction mixture. The mixture was heated to 90 °C for 6 h under nitrogen. After the reaction was complete, the reaction mixture was

dx.doi.org/10.1021/cm2016824 |*Chem. Mater.* 2011, 23, 4038–4044

extracted with chloroform and water. The organic layer was dried with anhydrous $MgSO_4$ and filtered. The solvent was removed by evaporation. Recrystallization of the residue from $CHCl_3$/MeOH afforded a white product: 50% yield, ^{1}H NMR (300 MHz, $CDCl_3$): 7.07(s, 2H), 6.99−6.90(m, 4H), 2.24(s, 6H).

Synthesis of Compound ***3b***. Compound **2b** (1 g, 3.0 mmol), $KMnO_4$ (2.35 g, 1.50 mmol), and 16 mL pyridine were mixed. The reaction mixture was stirred using a mechanical stirrer and refluxed. $KMnO_4$ (1.5 g, 9.5 mmol) in 3 mL of water was added to the reaction mixture once every 30 min for a total of four such additions. The reaction mixture was further refluxed. After 5 h, 20 mL of water was added, and refluxing was continued overnight. The MnO_4 precipitate was removed by hot filtering and washed with boiling water. The filtrate was filtered through Celite. The filtrate was concentrated, and acid was recovered as concentrated HCl. The white product was dried overnight at 80 °C in a vacuum oven: 98% yield, ^{1}H NMR (300 MHz, DMSO-d_6): 13.14(Br, 2H), 7.79(s, 2H), 7.39−7.04(m, 6H).

Synthesis of Compound ***3c***. Compound **2b** (1.3 g, 3.5 mmol), $KMnO_4$ (2.8 g, 17.5 mmol), and 25 mL pyridine were mixed. The reaction mixture was stirred using a mechanical stirrer and refluxed. $KMnO_4$ (1.5 g, 9.5 mmol) in 3 mL water was added to the reaction mixture once every 30 min for a total of four additions. The reaction mixture was further refluxed. After 5 h, 20 mL of water were added and refluxing was continued overnight. The MnO_4 precipitate was removed by hot filtering and washed with boiling water. The filtrate was filtered through Celite. The filtrate was concentrated, and acid was recovered as concentrated HCl. The white product was dried overnight at 80 °C in a vacuum oven: 98% yield, ^{1}H NMR (300 MHz, DMSO-d_6): 13.25(Br, 2H), 7.81−7.69(m, 2H), 7.43−7.38(m, 4H).

Synthesis of Compound DiF-IF-dione. Small portions of compound **3b** (0.4 g, 1.0 mmol) were dissolved in 20 mL of H_2SO_4. The red mixture was stirred for 12 h at 50 °C and then poured over ice. The red precipitate was filtered and washed with water. The solid was then stirred in a K_2CO_3 solution for 3 h, filtered under suction, and THF was used for recrystallization, which yielded a red solid: 72% yield, IR (KBr): 1706, 1602, 1482, 1426, 1380, 1175, 1137, 1092, 850, 817, 782, 630 cm^{-1} MS/EI: m/e 354 (M^+). Anal. Calcd. For $C_{20}H_6F_4O_2$: C, 67.81; H, 1.71; O, 9.03. Found: C, 67.76; H, 1.80; O, 9.08.

Synthesis of Compound TriF-IF-dione. Small portions of compound **3b** (0.5 g, 1.1 mmol) were dissolved in 20 mL of H_2SO_4. The red mixture was stirred for 12 h at room temperature and then poured over ice. The red precipitate was filtered and washed with water. The solid was then stirred in a K_2CO_3 solution for 3 h, filtered under suction, and THF was used for recrystallization, which yielded a red solid: 70% yield, IR (KBr): 1707, 1620, 1511, 1472, 1273, 1250, 1124, 1085, 887, 817, 785, 662 cm^{-1} MS/EI: m/e 390 (M^+). Anal. Calcd. For $C_{20}H_4F_6O_2$: C, 61.56; H, 1.03; O, 8.20. Found: C, 61.53; H, 1.01; O, 8.30.

2.2. Material Characterization. Fast atom bombardment (FAB) mass spectra were recorded on a JEOL Model JMS-AX505WA, HP5890 series II system. Elemental analysis was recorded on CE Instruments systems (Models EA1110 and EA1112). UV−vis absorption spectra were obtained using a Hewlett-Packard Model HP 8453 UV−vis−NIR spectrometer. The reduction potentials of the compounds were determined by cyclic voltammetry (CV), using an AUTOLAB/PGSTAT128N model system with a scanning rate of 20 mV/s. The synthesized materials were used to coat indium tin oxide (ITO) to form a working electrode, a saturated $Ag/AgNO_3$ was used as a reference electrode, and dry dimethylformamide (DMF) with 0.1 M tetrabutylammonium perchlorate (TBAP) was used as the electrolyte. Ferrocene was used to calibrate the potential and for the reversibility criteria.

2.3. Device Fabrication. OFETs were fabricated using a highly doped *n*-type Si wafer with a thermally grown 300-nm-thick oxide layer as the substrate. The wafer served as the gate electrode, whereas the oxide layer acted as a gate insulator. Prior to treating the silicon oxide surface, the wafer was cleaned in piranha solution for 30 min at 100 °C, then washed with copious amounts of distilled water. Thin PS layers were spincast onto SiO_2/Si substrates (t = 15.2 nm). MonoF-IF-dione, DiF-IF-dione, and TriF-IF-dione films, 100 nm thick, were deposited from a quartz crucible onto the PS-coated substrates at a rate of 0.4 Å/s using an organic molecular beam deposition (OMBD) system. The devices were completed by evaporating Au through a shadow mask to define the source and drain contact electrodes on the indenofluorenedione films. Transistor current−voltage characteristics were measured using Keithley source/measure units (Models 2400 and 236) at room temperature under ambient conditions or vacuum (10^{-5} Torr) in a dark environment.

3. RESULTS AND DISCUSSION

The electronic properties of the indenofluorenediones with different numbers of fluorine substituents were investigated using UV−vis absorption spectroscopy and cyclic voltammetry (CV). The highest occupied molecular orbital (HOMO) and LUMO positions are crucial to understand the differences in the OFET electrical and environmental stabilities.[37] Figure S1 in the Supporting Information shows the UV−vis spectra of the indenofluorenediones. MonoF-IF-dione displayed three major absorption peaks—at 289, 314, and 329 nm—in solution (see Figure S1(a) in the Supporting Information). DiF-IF-dione and TriF-IF-dione showed similar absorption maxima at 280, 321, and 337 nm. The structured absorption bands in solution were also observed in the solid state (see Figure S1(b) in the Supporting Information). However, the solid-state absorption bands were red-shifted, compared to the corresponding bands in solution, which indicated an increase in the conjugation length in the solid state. The increase in conjugation length may have been due to the more-planar conformations of the π-stacked compounds in the solid state.[36] The HOMO−LUMO optical band gaps obtained from the onset of absorption were 3.43 eV for MonoF-IF-dione, 3.24 eV for DiF-IF-dione, and 3.20 eV for TriF-IF-dione. The energy levels of MonoF-IF-dione, DiF-IF-dione, and TriF-IF-dione were estimated using electrochemical measurements (see Figure S2 in the Supporting Information). The LUMO levels were calculated from the electrochemical reduction potentials.[38] The LUMO level of MonoF-IF-dione was found to be −3.38 eV, which decreased by 0.15 eV upon the substitution of three electronegative fluorine groups. This result was consistent with trends observed previously for pentacene and perfluoropentacene.[39] The HOMO levels were estimated from the optical band gaps (E_g) and the LUMO levels. The electronic structures of the indenofluorenediones are summarized in Table 1.

Field-effect transistors (FETs) based on the indenofluorenediones with different numbers of fluorine substituents were fabricated on heavily doped *n*-type Si substrates. A thermally grown 300-nm-thick SiO_2 layer served as the gate dielectric, which was modified using a 15.2-nm-thick polystyrene (PS) interlayer to reduce electron trapping by the silanol groups on SiO_2.[40] Figures 1a and 1c show the transfer characteristics (drain current−gate voltage, I_D vs V_G) of MonoF-IF-dione, DiF-IF-dione, and TriF-IF-dione FETs with Al/LiF and Au source and drain contacts, respectively, at a drain voltage (V_D) of 60 V. All devices in this study were found to be well-operated as *n*-type transistors. On/off current ratios of the devices exceeded 10^5. The threshold voltage (V_{th}) of the TriF-IF-dione FETs with Au contacts was determined to be 9.2 V, compared with the values of

Table 1. Optical Properties of the MonoF-IF-dione, DiF-IF-dione, and TriF-IF-dione

	UV−vis (nm)					
	solution[a]	film	E_{red}^{onset} (V)	LUMO[b] (eV)	HOMO[c] (eV)	E_g[d] (eV)
MonoF-IF-dione	289, 314, 329	307, 314, 340	−1.02	−3.38	−6.81	3.43
DiF-IF-dione	285, 321, 337	305, 356, 372	−0.97	−3.43	−6.67	3.24
TriF-IF-dione	285, 319, 334	308, 358, 373	−0.87	−3.53	−6.73	3.20

[a] THF solution (1×10^{-4} M). [b] LUMO = E_{red}^{onset} + 4.4 eV. [c] HOMO level was determined from the LUMO level and the optical band gap. [d] The optical band gap was derived from the absorption edge of the thin film.

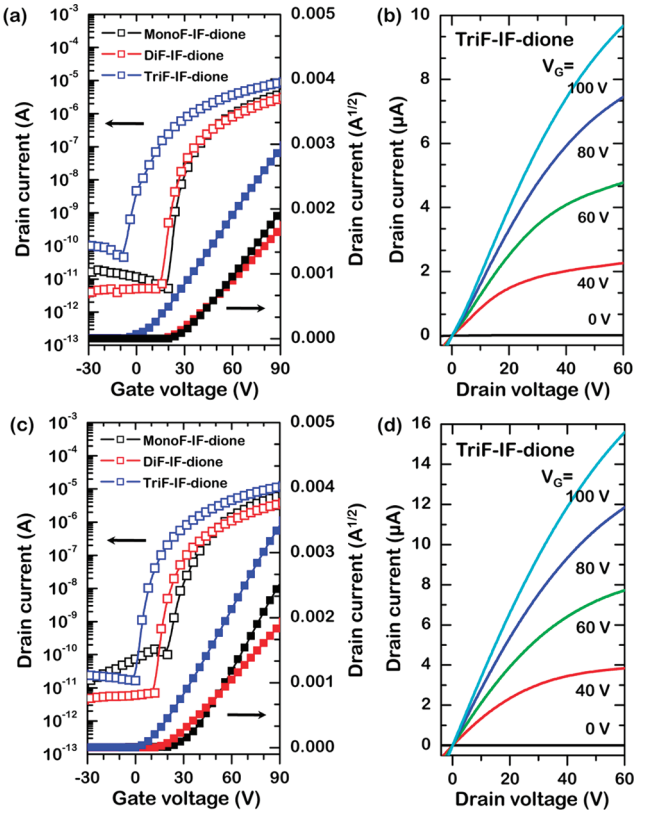

Figure 1. Transfer (I_D vs V_G) and output characteristics (I_D vs V_D) of MonoF-IF-dione, DiF-IF-dione, and TriF-IF-dione FETs, based on (a and b) LiF/Al and (c and d) Au source/drain contacts.

22.2 V for DiF-IF-dione and 32.1 V for MonoF-IF-dione FETs. This was due to the decrease in the LUMO levels for higher numbers of substituted fluorine groups.[41] The electron mobilities of each FET were calculated in the saturation regime (V_D = 60 V) using the relationship $I_D = C_i\mu W(V_G - V_{th})^2/(2L)$, where W and L are the channel width and length, respectively, C_i is the specific capacitance of the gate dielectric (11 nF/cm^2), and μ is the electron mobility. The MonoF-IF-dione, DiF-IF-dione, and TriF-IF-dione FETs with LiF/Al contacts showed electron mobilities of 0.07, 0.05, and 0.09 cm^2/(V s), respectively. No difference in the device performance was found for higher numbers of fluorine substituents. The transistor performances are summarized in Table 2. The crystalline nanostructures and surface morphologies of all samples were also analyzed using two-dimension (2D) grazing-incidence X-ray diffraction (GIXD) and atomic force microscopy (AFM) (see Figures S3 and S4 in the Supporting Information).

Table 2. Electrical Properties of the MonoF-dione FETs, DiF-IF-dione, and TriF-dione FETs, Based on LiF/Al and Au Source/Drain Contacts

	field-effect mobility (cm^2/(V s))	ON/OFF current ratio	V_{th} (V)
MonoF-IF-dione			
LiF/Al	0.07 (±0.03)	6.9 (±2.4) × 10^5	31.7 (±7.9)
Au	0.14 (±0.02)	1.2 (±0.5) × 10^5	32.1 (±8.5)
DiF-IF-dione			
LiF/Al	0.05 (±0.02)	4.3 (±0.7) × 10^5	26.1 (±6.1)
Au	0.07 (±0.03)	5.4 (±1.3) × 10^5	22.2 (±4.8)
TriF-IF-dione			
LiF/Al	0.09 (±0.02)	1.8 (±0.6) × 10^5	4.7 (±2.6)
Au	0.16 (±0.04)	6.8 (±3.5) × 10^5	9.2 (±5.3)

Note that the Au contacts yielded FETs with much higher electron mobilities of 0.14, 0.07, and 0.16 cm^2/(V s) for MonoF-IF-dione, DiF-IF-dione, and TriF-IF-dione, respectively, as discussed below. Figures 1b and 1d show typical output characteristics (I_D vs V_D) of TriF-IF-dione FETs with Al/LiF and Au source and drain contacts, respectively. The maximum I_D value of TriF-IF-dione FETs with Au contacts in the saturation regime (V_D = 60 V) was higher than that of devices with LiF/Al contacts.

The effects of LiF/Al and Au contacts on the OFET performance were quantified by measuring the channel length dependence of the resistance of TriF-IF-dione FETs at small drain voltages by analyzing the output characteristics.[42] The contact resistance ($R_{contact}$) was obtained from the L = 0 intersection of the measured device resistance at each gate voltage, as indicated by the following equation:

$$R_{total} = R_c + \frac{L}{W[\mu_i C_i(V_G - V_{th,i})]}$$

where μ_i and $V_{th,i}$ are the intrinsic field-effect mobility and the threshold voltage, respectively. R_{total} is the total resistance. The channel width-normalized total resistance of the TriF-IF-dione FETs with LiF/Al and Au contacts is plotted as a function of the channel length for each V_G value, as shown in Figure 2a. The y-intercept of the $R_{total}W$ vs L plot was used to evaluate the contact resistance, as a function of gate voltage (Figure 2b). The channel-width-normalized contact resistance of the TriF-IF-dione FETs with LiF/Al contacts decreased from 0.25 to 0.14 MΩ cm as the V_G value was varied from 40 V to 100 V. In contrast, the contact resistance of the TriF-IF-dione FETs with Au contacts varied from 0.09 MΩ cm to 0.01 MΩ cm. The contact resistance of devices with Au contacts was reduced more than 3-fold relative to devices with LiF/Al contacts.

dx.doi.org/10.1021/cm2016824 |Chem. Mater. 2011, 23, 4038–4044

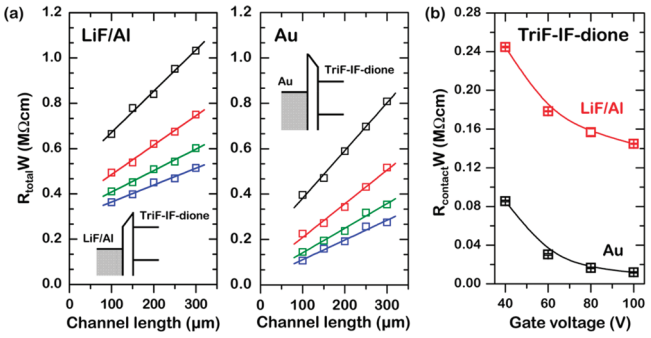

Figure 2. (a) Channel-width-normalized R_{total}, as a function of the channel length at gate voltages in the range of 40−100 V at intervals of 20 V, for TriF-IF-dione FETs, based on LiF/Al and Au source/drain contacts. (b) Channel-width-normalized contact resistance ($R_{contact}$), as a function of gate voltage.

LiF/Al contacts are widely used in *n*-type transistors, because of their low work function. Au contacts in TriF-IF-dione FETs yielded better electrical performances, even though the work function of Au is higher than that of LiF/Al. This may be due to a vacuum level shift at the semiconductor/metal interface.[43] The interfacial potential of the LiF/Al contacts shifted in a direction that imposed a negative charge on the TriF-IF-dione molecules, which increased the electron injection barrier from LiF/Al to TriF-IF-dione (see inset of Figure 2a). In contrast, Au contacts shifted in the opposite direction as the interfacial dipoles, leading a downward shift in the semiconductor energy level and a reduced electron injection barrier (inset of Figure 2b). A lower electron injection barrier for Au contacts enables the easy fabrication of complementary circuits with both *p*-type and *n*-type semiconductors, because of the use of the same metal in the *p*-type transistors.

The electrical stabilities of MonoF-IF-dione and TriF-IF-dione FETs were obtained by measuring the threshold voltage (V_{th}), as a function of time under bias stress (see Figure 3). A sustained gate voltage of 50 V was applied over a period of 90 min. The measurement was performed under vacuum (10^{-5} Torr) to exclude the effects of semiconductor degradation in air. Remarkably, the V_{th} shift was much smaller for the TriF-IF-dione FETs than for the MonoF-IF-dione FETs, as shown in Figure 3a. The V_{th} shift was indicative of charge trapping instabilities in the transistors. The relative threshold voltage shifts (ΔV_{th}) of MonoF-IF-dione and TriF-IF-dione FETs are summarized in Figure 3b. The electrical stabilities of MonoF-IF-dione and TriF-IF-dione FETs were quantified by modeling the threshold voltage shift using a stretched exponential equation:[44]

$$\frac{V_{th} - V_{th,i}}{V_G - V_{th,i}} = 1 - \frac{1}{\{1 + \exp[(E_{th} - E_A)/(k_B T_0)]\}^{1/(\alpha - 1)}}$$

where $V_{th,i}$ is the initial V_{th}, E_A a typical activation energy for trap creation, $k_B T_0$ the slope of the activation energy distribution, and α a constant. E_{th} corresponds to the thermalization energy, defined by $k_B T \ln(\nu t)$. Here, k_B and ν are the Boltzmann constant and the attempt-to-escape frequency, respectively. The curves that described the dependence of the shift in V_{th} on the stress time were clearly fit by this equation, as shown in Figure 3c. Here, the fitting parameters were E_A, $k_B T_0$, ν, and α. The optimal fit yielded values for ν and α of 10^5 Hz and 1.5, respectively, which agreed well with previously reported values.[44] The parameters

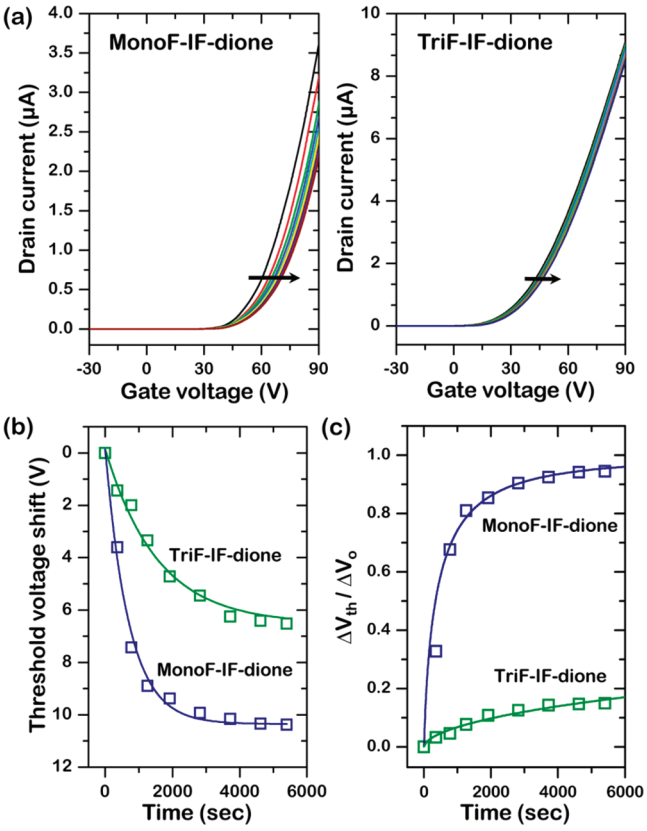

Figure 3. (a) Evolution of the linear transfer curves of MonoF-IF-dione FETs and TriF-IF-dione FETs, based on Au source/drain contacts as a function of bias stress time (0−90 min). The gate bias during stress was 50 V. (b) The relative threshold voltage shift (V_{th}) of MonoF-IF-dione FETs and TriF-IF-dione FETs, as a function of stress time. (c) Plot of $\Delta V_{th}/\Delta V_0$ versus bias stress time for the MonoF-IF-dione FETs and TriF-IF-dione FETs. Solid curves were fit to a stretched exponential equation.

Table 3. E_A and $k_B T$ of the MonoF-dione FETs and TriF-dione FETs, Based on Au Source/Drain Contacts

	Value	
parameter	MonoF-dione	TriF-dione
E_A (eV)	0.477 (±0.001)	0.629 (±0.013)
$k_B T_0$ (eV)	0.033 (±0.002)	0.046 (±0.005)

associated with the activation energy (E_A) and $k_B T$ are summarized in Table 3. The fits yielded E_A values of 0.477 eV for MonoF-IF-dione FETs and 0.629 eV for TriF-IF-dione FETs. The small values of ΔV_{th} for TriF-IF-dione FETs were attributed to higher activation energies for trap creation. The use of TriF-IF-dione, which is a more-electron-depleted semiconductor, reduces the possibility for the electrons to be trapped, since they are located on lower energy.

We examined the long-term environmental stability of MonoF-IF-dione and TriF-IF-dione FETs stored in air in darkness for 1 month. Figure 4 shows the changes in the electron mobilities of MonoF-IF-dione and TriF-IF-dione FETs, as a function of time. MonoF-IF-dione FETs exhibited a dramatic decrease in the electron mobilities from 0.14 $cm^2/(V\ s)$ to 0.003 $cm^2/(V\ s)$

dx.doi.org/10.1021/cm2016824 |*Chem. Mater.* 2011, 23, 4038–4044

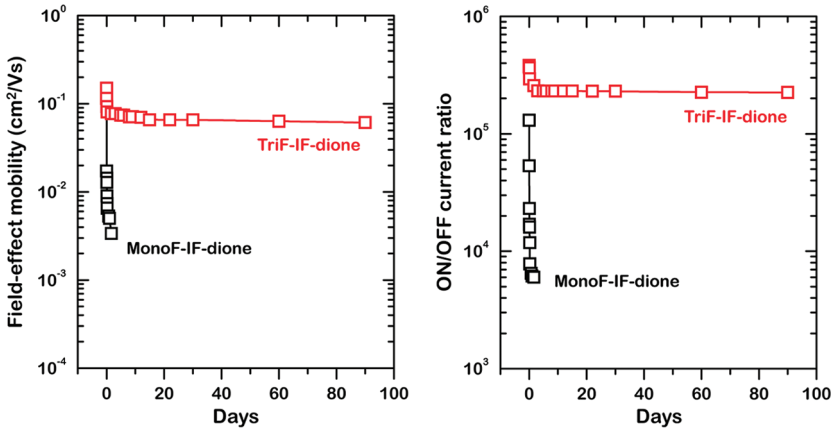

Figure 4. Long-term environmental stability of MonoF-IF-dione FETs and TriF-IF-dione FETs based on Au source/drain contacts, stored in air in darkness for 1 month.

after 40 h of storage in air. After 40 h, the devices showed no gate effects. However, the electron mobilities of TriF-IF-dione FETs decreased from 0.15 to 0.07 after 40 min of storage in air, but showed negligible changes, even after 3 months. This trend was observed in the on/off current ratio (see Figure 4). The high environmental stability of TriF-IF-dione FETs arose from the lower LUMO levels of TriF-IF-dione, relative to the LUMO of MonoF-IF-dione.

4. CONCLUSIONS

In summary, indenofluorenediones with different numbers of fluorine substituents (MonoF-IF-dione, DiF-IF-dione, and TriF-IF-dione) were synthesized for use in high-performance stable *n*-type organic field-effect transistors (OFETs). TriF-IF-dione FETs with Au source/drain contacts fabricated atop polystyrene (PS) substrates showed excellent device performance, with a field-effect mobility of 0.16 $cm^2/(V\ s)$, an on/off current ratio of 10^6, and a threshold voltage of 9.2 V. Moreover, the TriF-IF-dione OFETs yielded excellent electrical and environmental stabilities, because of the low lowest unoccupied molecular orbital (LUMO) levels, compared to the LUMOs of MonoF-IF-dione FETs.

■ ASSOCIATED CONTENT

Ⓢ Supporting Information. This material is available free of charge via the Internet at http://pubs.acs.org.

■ AUTHOR INFORMATION

Corresponding Author

*E-mail addresses: jhcho94@ssu.ac.kr (J.H.C.) and hahapark@catholic.ac.kr (J.-W.P.).

Author Contributions

⊥Y. I. Park and J. S. Lee contributed equally to this work.

■ ACKNOWLEDGMENT

This research was supported by Basic Science Research Program through the National Research Foundation of Korea (NRF) funded by the Ministry of Education, Science and Technology (No. 20100026294).

■ REFERENCES

(1) Street, R. A.; Wong, W. S.; Ready, S. E.; Chabinyc, I. L.; Arias, A. C.; Limb, S.; Salleo, A.; Lujan, R. *Mater. Today* **2006**, *9*, 32.
(2) Sirringhaus, H. *Adv. Mater.* **2005**, *17*, 2411.
(3) Sekitani, T.; Takamiya, M.; Noguchi, Y.; Nakano, S.; Kato, Y.; Sakurai, T.; Someya, T. *Nat. Mater.* **2007**, *6*, 413.
(4) Liu, S.; Briseno, A. L.; Mannsfeld, S. C. B.; You, W.; Locklin, J.; Lee, H. W.; Xia, Y.; Bao, Z. *Adv. Funct. Mater.* **2007**, *17*, 2891.
(5) Kim, C.; Facchetti, A.; Marks, T. J. *Science* **2007**, *318*, 76.
(6) Braga, D.; Horowitz, G. *Adv. Mater.* **2009**, *21*, 1473.
(7) Park, K.; Park, S. H.; Kim, E.; Kim, J.-D.; An, S.-Y.; Lim, H. S.; Lee, H. H.; Kim, D. H.; Ryu, D. Y.; Lee, D. R.; Cho, J. H. *Chem. Mater.* **2010**, *22*, 5377.
(8) Gundlach, D. J.; Royer, J. E.; Park, S. K.; Subramanian, S.; Jurchescu, O. D.; Hamadani, B. H.; Moad, A. J.; Kline, R. J.; Teague, L. C.; Kirillov, O.; Richter, C. A.; Kushmerick, J. G.; Richter, L. J.; Parkin, S. R.; Jackson, T. N.; Anthony, J. E. *Nat. Mater.* **2008**, *7*, 216.
(9) Zaumseil, J.; Sirringhaus, H. *Chem. Rev.* **2007**, *107*, 1296.
(10) Bao, Z.; Dodabalapur, A.; Lovinger, A. J. *Appl. Phys. Lett.* **1996**, *69*, 4108.
(11) Katz, H. E.; Bao, Z.; Gilat, S. L. *Acc. Chem. Res.* **2001**, *14*, 359–369.
(12) Jung, T.; Yoo, B.; Wang, L.; Jones, B. A.; Facchetti, A.; Wasielewski, M. R.; Marks, T. J.; Dodabalapur, A. *Appl. Phys. Lett.* **2006**, *88*, 183102.
(13) De Vusser, S.; Steudel, S.; Myny, K.; Genoe, J.; Heremans, P. *Appl. Phys. Lett.* **2006**, *88*, 162116.
(14) Klauk, H.; Zschieschang, U.; Pflaum, J.; Halik, M. *Nature* **2007**, *445*, 745.
(15) Yoo, B.; Madgavkar, A.; Jones, B. A.; Nadkarni, S.; Facchetti, A.; Dimmler, D.; Wasielewski, M. R.; Marks, T. J.; Dodabalapur, A. *IEEE Electron Device Lett.* **2006**, *27*, 737–739.
(16) Newman, C. R.; Frisbie, C. D.; Filho, D. A.; da, S.; Brédas, J.-L.; Ewbank, P. C.; Mann, K. R. *Chem. Mater.* **2004**, *16*, 4436–4451.
(17) Chua, L.-L.; Zaumseil, J.; Chang, J.-F.; Ou, E. C.-W.; Ho, P. K.-H.; Sirringhaus, H.; Friend, R. H. *Nature* **2005**, *434*, 194–199.
(18) Facchetti, A.; Letizia, J.; Yoon, M.-H.; Mushrush, M.; Katz, H. E.; Marks, T. J. *Chem. Mater.* **2004**, *16*, 4715–4724.
(19) Zhang, M.; Tsao, H. N.; Pisula, W.; Yang, C.; Mishra, A. K.; Müellen, K. *J. Am. Chem. Soc.* **2007**, *129*, 3472–3473.
(20) Coropceanu, V.; Cornil, J.; Da Silva Filho, D. A.; Olivier, Y.; Silbey, R.; Brédas, J.-L. *Chem. Rev.* **2007**, *107*, 2165.
(21) Cai, X.; Burand, M. W.; Newman, C. R.; da Sliva Filho, D. A.; Pappenfus, T. M.; Bader, M. M.; Brédas, J.-L.; Mann, K. R.; Frisbie, C. D. *J. Phys. Chem. B* **2006**, *110*, 14590–14597.
(22) Jones, B. A.; Ahrens, M. J.; Yoon, M.-H.; Facchetti, A.; Marks, T. J.; Wasielewski, M. R. *Angew. Chem., Int. Ed.* **2004**, *43*, 6363–6366.

(23) Bao, Z. *Adv. Mater.* **2000**, *12*, 227–230.
(24) Frankevich, E.; Maruyama, Y.; Ogata, H. *Chem. Phys. Lett.* **1993**, *214*, 39.
(25) Meijer, E. J.; De Leeuw, D. M.; Setayesh, S.; van Veenendaal, E.; Huisman, B. H.; Blom, P. W. M.; Hummelen, J. C.; Scherf, U.; Klapwijk, T. M. *Nat. Mater.* **2003**, *2*, 678.
(26) Malenfant, P. R. L.; Dimitrakopoulos, C. D.; Gelorme, J. D.; Kosbar, L. L.; Graham, T. O.; Curioni, A.; Andreoni, W. *Appl. Phys. Lett.* **2002**, *80*, 2517.
(27) Katz, H. E.; Lovinger, A. J.; Johnson, J.; Kloc, C.; Siegrist, T.; Li, W.; Lin, Y. Y.; Dodabalapur, A. *Nature* **2000**, *404*, 478.
(28) Facchetti, A.; Mushrush, M.; Yoon, M.-H.; Hutchison, G. R.; Ratner, M. A.; Marks, T. J. *J. Am. Chem. Soc.* **2004**, *126*, 13859.
(29) Bao, Z.; Lovinger, A. J.; Brown, J. *J. Am. Chem. Soc.* **1998**, *120*, 207.
(30) Ye, R.; Baba, M.; Oishi, Y.; Mori, K.; Suzuki, K. *Appl. Phys. Lett.* **2005**, *86*, 253505.
(31) Yoon, M.-H.; DiBenedetto, S.; Facchetti, A.; Marks, T. J. *J. Am. Chem. Soc.* **2005**, *127*, 1348–1349.
(32) Katz, H. E.; Siegrist, T.; Schön, J. H.; Kloc, C.; Batlogg, B.; Lovinger, A. J.; Johnson, J. *ChemPhysChem* **2001**, *3*, 167–172.
(33) Ahrens, M. J.; Fuller, M. J.; Wasielewski, M. R. *Chem. Mater.* **2003**, *15*, 2684–2686.
(34) Chen, H. Z.; Ling, M. M.; Mo, X.; Shi, M. M.; Wang, M.; Bao, Z. *Chem. Mater.* **2007**, *19*, 816.
(35) Nakagawa, T.; Kumaki, D.; Nishida, J.; Tokito, S.; Yamashita, Y. *Chem. Mater.* **2008**, *20*, 2615.
(36) Vak, D.; Lim, B.; Lee, S.; Kim, D. *Org. Lett.* **2005**, *19*, 4229.
(37) Oh, J. H.; Suraru, S.-L.; Lee, W.-Y.; Könemann, M.; Höffken, H. W.; Röger, C.; Schmidt, R.; Chung, Y.; Chen, W.-C.; Würthner, F.; Bao, Z. *Adv. Func. Mater.* **2010**, *20*, 2148.
(38) Tonzola, C. J.; Alam, M. M.; Kaminsky, W.; Jenekhe, S. A. *J. Am. Chem. Soc.* **2003**, *125*, 13548.
(39) Sakamoto, Y.; Suzuki, T.; Kobayashi, M.; Gao, Y.; Fukai, Y.; Inoue, Y.; Sato, F.; Tokito, S. *J. Am. Chem. Soc.* **2004**, *126*, 8138.
(40) Yoon, M.-H.; Yan, H.; Facchetti, A.; Marks, T. J. *J. Am. Chem. Soc.* **2005**, *127*, 10395.
(41) Jones, B. A.; Facchetti, A.; Wasielewski, M. R.; Marks, T. J. *J. Am. Chem. Soc.* **2007**, *129*, 15259.
(42) Sirringhaus, H.; Tessler, N.; Thomas, D. S.; Brown, P. J.; Friend, R. H. *Advances in Solid State Physics*; Springer: Berlin, 1999.
(43) Wada, H.; Shibata., K.; Bando, Y.; Mori, T. *J. Mater. Chem.* **2008**, *18*, 4165.
(44) Suemori, K.; Uemura, S.; Yoshida, M.; Hoshino, S.; Takada, M.; Kodzasa, T.; Kamata, T. *Appl. Phys. Lett.* **2007**, *91*, 192112.